



## Ultrasonic time-reversal-based super resolution imaging for defect localization and characterization

Chengguang Fan<sup>\*</sup>, Sunquan Yu, Bin Gao, Yong Zhao, Lei Yang

College of Aerospace Science and Engineering, National University of Defense Technology, Changsha, 410073, PR China



### ARTICLE INFO

**Keywords:**  
Super resolution imaging  
Full matrix capture  
Defect characterization  
Extended target  
Time reversal

### ABSTRACT

In this paper, time reversal with multiple signal classification (TR-MUSIC) and its phase-coherent form (PC-MUSIC), the two typical ultrasonic time-reversal-based super resolution imaging techniques, have been introduced and explored to image defects in metallic samples. The principles for super resolution imaging technique and defect characterization based on ultrasonic image have been presented firstly. And then both TR-MUSIC and PC-MUSIC are tested with experimental ultrasonic array data acquired from the metallic samples including defects using the full matrix capture (FMC) process. Here, if the size of defect is smaller than the central ultrasonic wavelength, the defect can be regarded as point-like target. On the contrary, if the size of defect is larger than the central ultrasonic wavelength, it can be regarded as extended target. The comparison on super resolution imaging for point-like and extended targets has been investigated. For point-like targets, TR-MUSIC as well as PC-MUSIC can distinguish and locate the position, and the overall performance of TR-MUSIC is better than that of PC-MUSIC. For extended target, TR-MUSIC can only determine the area where the defect occurs. PC-MUSIC can distinguish and assess the length of extended target parallel to the array, the lowest error is 9.62% when the dimension of signal subspace is set to be 10 for the case considered. In addition, the defect characterization based on ultrasonic super-resolved image has been studied, and a sizing strategy is introduced. The length and angle of extended targets oblique to the array can be obtained from the PC-MUSIC images. The worst errors for assessing the length and angel are 9.14% and 13.3% respectively. And for the cases considered in the experiment, the longer the length of extended target, the smaller the error.

### 1. Introduction

Ultrasonic phased arrays have been widely used in the area of Nondestructive Evaluation (NDE) due to their increased flexibility over traditional single element transducer. There are various kinds of ultrasonic array transducers, in which 1-D linear arrays are by far the most widespread in industrial field [1]. For a given linear array, full matrix capture (FMC) is the typical approach to collect the ultrasonic array data for offline post-processing techniques [2]. Different imaging techniques can be utilized to post-process the same FMC data in order to obtain the ultrasonic image of the tested object, one of which is time-reversal-based imaging technique [3]. And the super-resolved technique frequently used in ultrasonic is time-reversal with multiple signal classification (TR-MUSIC) as well as its improved forms. TR-MUSIC was firstly utilized to locate the position of adjacent scatterers via simulated data [4]. It has also been experimentally demonstrated to locate the targets in water [5] as well as metallic block [6], the size of which is smaller than the

ultrasonic wavelength at the central frequency of array, termed point-like targets in this paper. The simulated and experimental results show that TR-MUSIC can break diffraction limit and achieve super resolution imaging. In addition, TR-MUSIC has been introduced to image the 34 mm long slot in a steel block, the size of which is larger than the central ultrasonic wavelength, termed extended target in this paper. The results show that TR-MUSIC can only extract some of the structural feathers of the slot [7]. In the field of medical imaging, TR-MUSIC was utilized to locate the spheres with different sizes. The experimental results show that these spheres can be located correctly, however, their shape information cannot be distinguished [8]. Actually, TR-MUSIC can only achieve super resolution imaging when the point-like targets are distributed along the direction perpendicular to that of the ultrasonic beam. Due to the axial elongation shown in the TR-MUSIC images, it has the poorly axial resolution. To solve the problem, PC-MUSIC, the phase coherent form of TR-MUSIC, has been introduced. Its performance has also been experimentally evaluated to correctly locate the point-like

\* Corresponding author.

E-mail address: [chengguangfannudt@163.com](mailto:chengguangfannudt@163.com) (C. Fan).

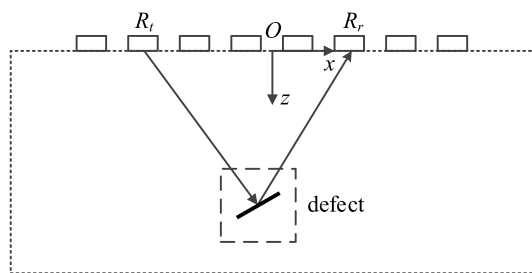


Fig. 1. The geometry of linear array.

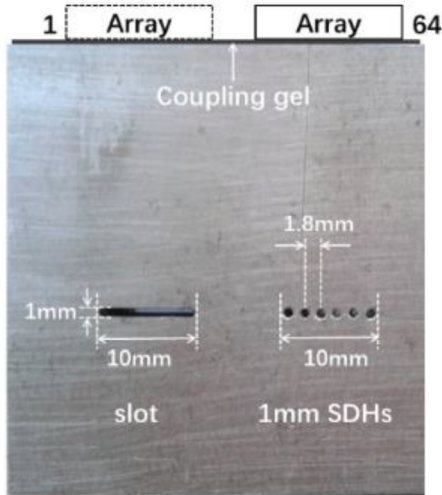


Fig. 2. Steel sample with SDHs and slot.

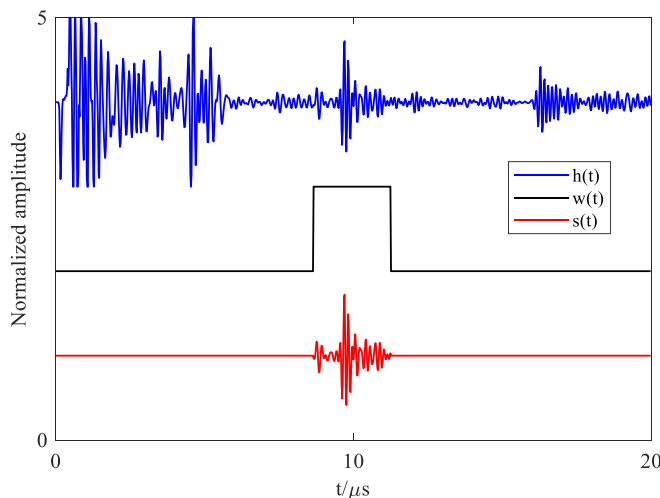


Fig. 3. Time domain signal preprocessing.

targets in the water tank [9] and tissue-mimicking phantoms [10]. On the other hand, the TR-MUSIC or MUSIC has been combined with Lamb wave for structural health monitoring (SHM) fields recently. A Lamb wave-based TR-MUSIC/DORT-MUSIC algorithm has been introduced to detect damage in metallic plates [11]. Ameliorated-multiple signal classification (Am-MUSIC) under a sparse sensor network has been utilized to achieve damage imaging in aluminum plate for in-suit SHM [12]. And its improved algorithm, frequency-domain MUSIC (F-MUSIC) has been studied to reduce computational complexity and enhance

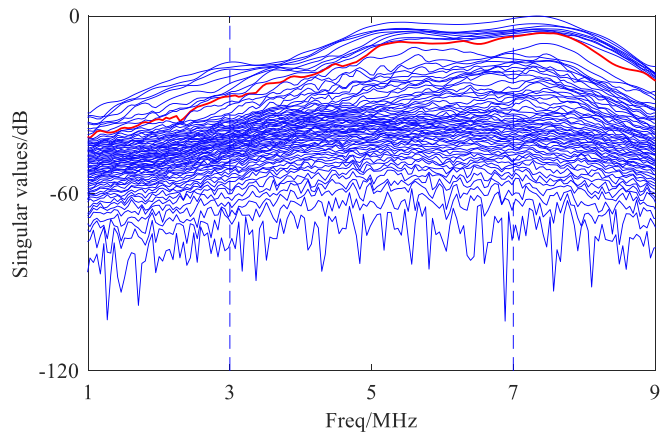


Fig. 4. Distribution of singular value amplitude in dB for the six SDHs.

imaging precision [13]. A focusing MUSIC algorithm has been proposed for baseline-free Lamb wave damage localization on isotropic materials, and its effectiveness has been experimentally verified [14]. In addition, a dispersive multiple signal classification algorithm for Lamb wave phased array based on FMC is developed to locate defects on an aluminum plate [15]. Thus the application of ultrasonic time-reversal-based super resolution imaging in the field of SHM will be an important research topic.

In reality, there has been a shift from NDE to quantitative NDE (QNDE) in the past few decades [16]. Defect characterization based on ultrasonic image is an important method in the QNDE area. There are some typical techniques to obtain ultrasonic image, such as scanning techniques, delay and sum techniques as well as super resolution techniques [17]. So far defect characterization based on ultrasonic super-resolved image is less investigated according to the published articles. Due to super-resolved capacity, the corresponding ultrasonic images show different characteristic. TR-MUSIC was applied to the simulated ultrasonic array inspection of small rough embedded planar defects to establish their characterization capabilities [18], and PC-MUSIC was introduced to assess the length of EDM lines parallel to the ultrasonic array [19]. The aim of this paper is to systematically evaluate the performance of time-reversal-based super resolution imaging for defect localization and characterization. Both TR-MUSIC and PC-MUSIC over a given frequency range are utilized to image point-like targets as well as extended targets in metallic samples. The comparison on super resolution imaging for point-like and extended targets has been studied, and a sizing strategy has also been introduced to assess the length and angle of extended targets oblique to the ultrasonic array.

## 2. Principles

Linear arrays are widely used in the area of industrial NDE. A linear array of  $N$  elements acting in the transmitter-receiver mode is employed, the geometry of which is shown in Fig. 1. Here, the Cartesian coordinate system will be used, where  $x$  and  $z$  represent positions in the lateral and depth directions respectively. Each element of the array can be excited and the backscattered signals are measured by all  $N$  elements.

### 2.1. Full matrix capture and signal preprocessing

Considering the situation that the linear array is in direct contact with the media containing defect as shown in Fig. 1. Ultrasonic array data can be collected via FMC process, which is an ultrasonic data acquisition process that utilizes phased array probes to capture the complete time domain signals for each transmit element  $R_t$  and receive element  $R_r$ . Therefore, for an array of  $N$  elements,  $N^2$  signals  $h_{ij}(t)$  ( $i, j$  ranging from 1 to  $N$ ) can be received. In reality, for time-reversal based

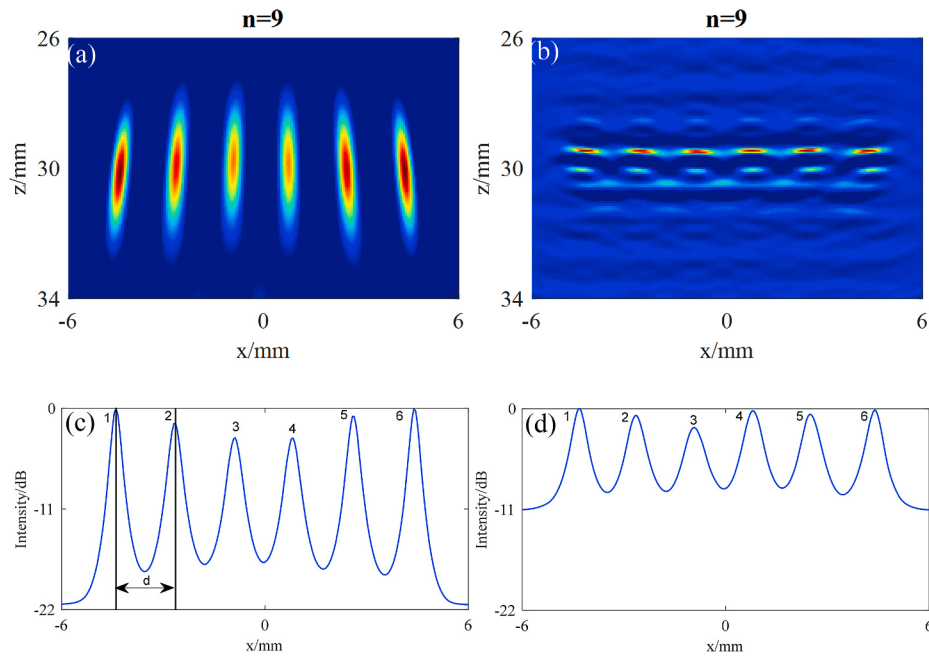


**Fig. 5.** (a)TR-MUSIC and (b) PC-MUSIC images for SDHs, and the lateral cross sections through the peaks of ultrasonic images obtained from (c)TR-MUSIC and (d) PC-MUSIC (all images are displayed with  $-12\text{dB}$  dynamic range).

**Table 1**  
The assessed distances for SDHs in steel sample.

Imaging techniques	Distance label	Actual value/mm	Assessed value/mm	Error
TR-MUSIC	$d_{12}$	1.8	1.757	0.043 (2.4%)
	$d_{23}$	1.8	1.7573	0.0427 (2.4%)
	$d_{34}$	1.8	1.7072	0.0928 (5.2%)
	$d_{45}$	1.8	1.7578	0.0422 (2.3%)
	$d_{56}$	1.8	1.807	0.007 (3.9%)
PC-MUSIC	$d_{12}$	1.8	1.657	0.143 (7.9%)
	$d_{23}$	1.8	1.7071	0.0929 (5.2%)
	$d_{34}$	1.8	1.7574	0.0426 (2.4%)
	$d_{45}$	1.8	1.6565	0.1435 (8.0%)
	$d_{56}$	1.8	1.908	0.108 (6.0%)

super resolution imaging technique, a window function is usually applied to extract the scattered signals related with defects in the pre-processing stage [20].

## 2.2. Super resolution imaging technique

TR-MUSIC and PC-MUSIC are two typical time-reversal-based super resolution imaging techniques, which are based on the ability to perform the singular value decomposition (SVD) of multi-static response matrix  $K$  to obtain the ultrasonic image of tested object. The matrix  $K$  can be directly constructed from the frequency spectrum of scattered signals related with defects [21].

For the given frequency component  $\omega$ , the SVD of  $K(\omega)$  is implemented to obtain singular values and corresponding singular vectors

$$K(\omega) = U(\omega)\Sigma(\omega)V^H(\omega), \quad (1)$$

where  $U(\omega)$  and  $V(\omega)$  are matrices whose columns are the singular vectors,  $\Sigma(\omega)$  is a diagonal matrix with singular values arranged in order of decreasing magnitude. The superscript  $H$  means complex conjugate transpose of the matrix.

The singular vectors are then divided into signal and noise subspaces based on the distributed characteristic of singular values. The matrix  $K(\omega)$  can be rewritten as

$$K(\omega) = [U_S(\omega) \ U_N(\omega)] \begin{bmatrix} \Sigma_S(\omega) & 0 \\ 0 & \Sigma_N(\omega) \end{bmatrix} \begin{bmatrix} V_S^H(\omega) \\ V_N^H(\omega) \end{bmatrix}, \quad (2)$$

where the subscripts  $S$  and  $N$  represent the signal and noise subspaces respectively. Note that there are several typical techniques to achieve the division, such as the 10% of the max singular value as well as the keen point of singular value spectrum in semi logarithmic scale can be regarded as the threshold [22–24]. However, up to now none of them can cover all the situations. The division technique depends on the specific detection scene.

A steering vector  $g(r, \omega)$  is defined to achieve the imaging process, and for each image pixel  $r$  in the imaging area, which is given by

$$g(r, \omega) = [G(R_1, r, \omega), G(R_2, r, \omega), \dots, G(R_N, r, \omega)]^T, \quad (3)$$

where  $R_l (l = 1, 2, \dots, N)$  are array element center positions. The superscript  $T$  means complex transpose of the matrix.

The function for time reversal based super resolution imaging technique [19], suited for TR-MUSIC and PC-MUSIC over the frequency range,  $\Delta\omega$ , is given by

$$I(r, \Delta\omega) = \left| \frac{1}{1 - \frac{1}{N_\omega} \sum_{\Delta\omega} A(r, \omega)} \right|, \quad (4)$$

where  $N_\omega$  is the number of frequency components within  $\Delta\omega$ .

The operator  $A(r, \omega)$  for TR-MUSIC and PC-MUSIC can be defined as

$$A(r, \omega) = \frac{g^H(r, \omega) U_S^H g(r, \omega)}{g(r, \omega)^2} = \frac{(g^H(r, \omega) U_S)(g^H(r, \omega) U_S)^H}{g(r, \omega)^2}, \quad (5a)$$

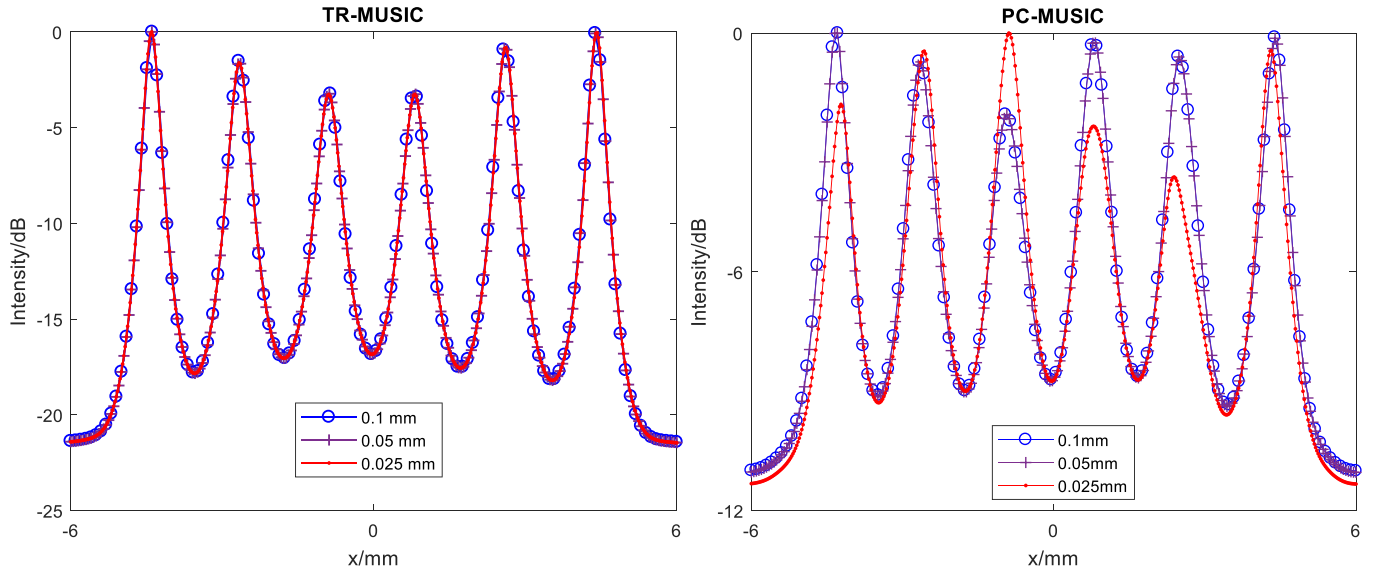


**Fig. 6.** Lateral cross sections through the peaks of TR-MUSIC and PC-MUSIC images under different grid size.

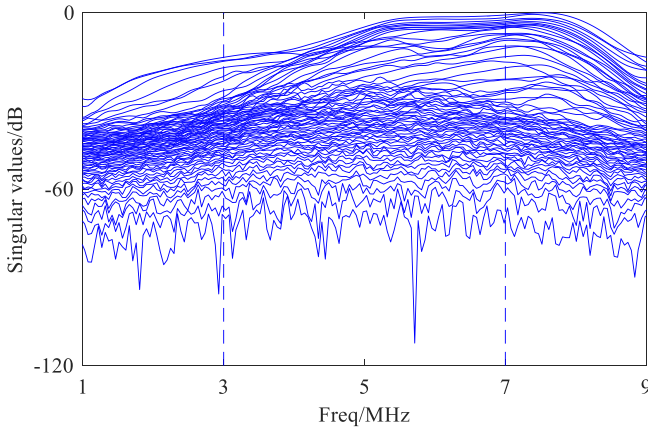


**Fig. 7.** Distribution of singular value amplitude in dB for slot.

$$A(r, \omega) = \frac{g^H(r, \omega) U_S U_S^T g^*(r, \omega)}{g(r, \omega)^2} = \frac{(g^H(r, \omega) U_S)(g^H(r, \omega) U_S)^T}{g(r, \omega)^2}. \quad (5b)$$

where the superscript \* means complex conjugate of the matrix.

### 2.3. Defect characterization based on ultrasonic images

It is often more intuitive to interpret ultrasonic imagery created from tested objects compared to the direct analysis of time domain signals. And imaging technique is an operator that transforms the time domain signals into intensity [25]. There are several methods to achieve defect measurement from ultrasonic images. Two of the main methods are measuring the size of an indication using an amplitude drop based technique applied to the image intensity, and measuring the distance between indications which correspond to each end of the defects within the imaging plane [17]. The size of an indication is commonly measured using the 6 dB drop technique. There are also some other techniques, such as point spread function (PSF) [26,27], array performance indicator (API) [2] as well as 6 dB boxing technique [28,29]. When measuring the distance between indications in an image, it is key to identify the defect extremities. Usually the peak position of each indication can be chosen as the defect extremity, and the distance between

different extremity can be calculated as the assessed size of defect.

The resolution of the ultrasonic image is an important estimator to compare various imaging techniques. The higher the resolution, the better the ultrasound image quality, and the defect localization and characterization can be better evaluated. Time-reversal-based super resolution imaging has the advantage of super-resolved capacity compared with most imaging techniques. A sizing strategy has been introduced and briefly illustrated here. For a super-resolved ultrasonic image, the image pixels (intensity  $\geq -6$  dB) have been searched firstly, note that 0 dB corresponds to the maximum intensity in the ultrasonic image. And then some false image pixels are removed. Thirdly, the position of defect extremity is searched and assessed. Lastly, the length and angle for extended target can be calculated, and the error can also be assessed. The detailed process will be illustrated in section 3.2.

### 3. Experimental demonstration

An experimental ultrasonic array system has been designed and built to capture the real data via FMC process. It consists of array controller (manufactured by Peak NDT Ltd., UK), 64-element linear array centered at 5 MHz (manufactured by Imasonic, France) and tested objects. Two metallic blocks with various defects are machined as the tested objects.

#### 3.1. Comparison on super resolution imaging for point-like and extended targets

A block of steel with six 1 mm side-drilled holes (SDHs) and a 1 mm by 10 mm slot is machined as the tested sample, which is shown in Fig. 2. Here, the 1 mm by 10 mm slot was machined using wire electrical discharge machining, starting from 1 mm starter hole drilled through the sample. The velocity of ultrasonic longitudinal wave in steel sample is 6150 m/s, so the wavelength  $\lambda_c$  at the central frequency of array, 5 MHz, is 1.2 mm. The diameter of SDH is smaller than the wavelength  $\lambda_c$ , meaning that these SDHs can be considered as point-like targets. Conversely, the length of slot is larger than the wavelength  $\lambda_c$ , it can be considered as the extended target.

Case one: Super resolution imaging for point-like targets.

The experimental ultrasonic array data acquired by FMC process includes 4096 time-domain signals due to the 64-element linear array utilized in the experiment. Taking the 32nd element as the transmitter and receiver, the collected ultrasonic signal  $h(t)$  is shown in Fig. 3, where various kinds of ultrasonic wave co-exist. A window function  $w(t)$  is

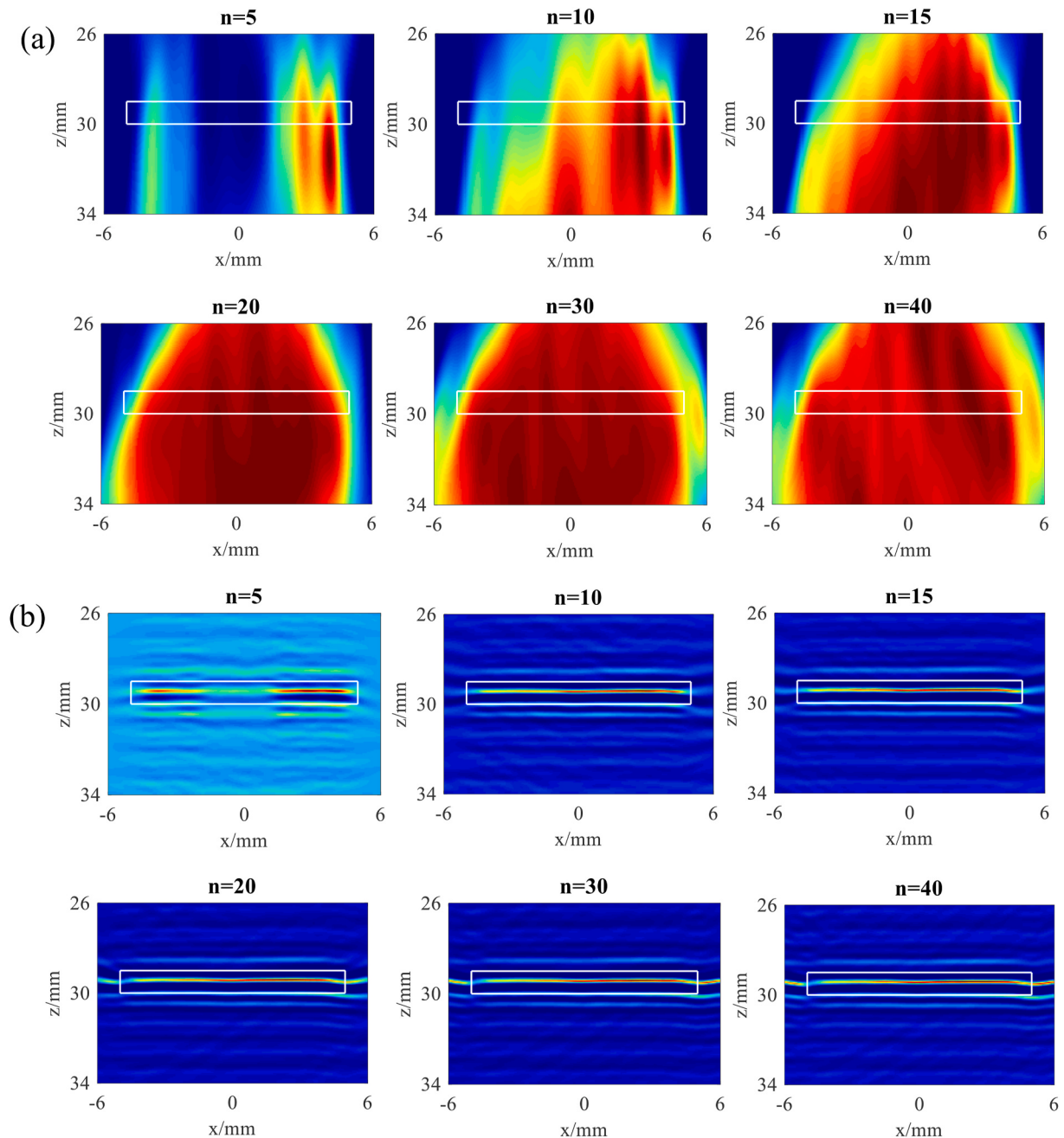


**Fig. 8.** (a) TR-MUSIC and (b) PC-MUSIC images for slot (all images are displayed with  $-12\text{dB}$  dynamic range).

employed to extract the scattered signal  $s(t)$  related with these SDHs. The same process can be implemented for each time domain signals belonging to the FMC data. The selection of the length of window function can refer to the author's previous research [20].

These scattered signals related with all the six SDHs can be used to construct the matrix  $K$  via time-frequency transform. At each frequency component  $\omega$ , the SVD of  $K(\omega)$  is implemented. The singular values and corresponding singular vectors can be obtained. Fig. 4 shows the distribution of singular value amplitude (in dB) over the frequency range from 1 MHz to 9 MHz.

In the experiment, the frequency band ranging from 3 MHz to 7 MHz, the middle frequency of which is equal to the central frequency of linear array, is considered. As shown in Fig. 4, it can be observed that the first nine singular values are larger than the remaining values over the given frequency band. So the dimension of signal subspace  $n$  is chosen to be 9 for each frequency component belonging to the given frequency band.

Note that the dimension is larger than the number of SDHs. The corresponding relation between the dimension of signal subspace and the number of point-like targets is no longer maintained in the experiment [5].

In the post-processing stage, both TR-MUSIC and PC-MUSIC are implemented over the frequency range from 3 MHz to 7 MHz in order to obtain the ultrasonic images of the six SDHs, as shown in Fig. 5(a) and Fig. 5(b). Here, the size of grid is set to be 0.05 mm in the rectangle imaging area. By comparing TR-MUSIC and PC-MUSIC images, it can be concluded that both methods can distinguish and locate the position of these point-like targets. For PC-MUSIC, there are some false targets, the intensity of which is smaller than  $-5\text{ dB}$ , and they may be caused by phase information in the imaging process.

To better quantitatively compare the performance of both methods for point-like targets, the lateral cross sections through the peaks of ultrasonic images have been extracted and shown in Fig. 5(c) and (d).

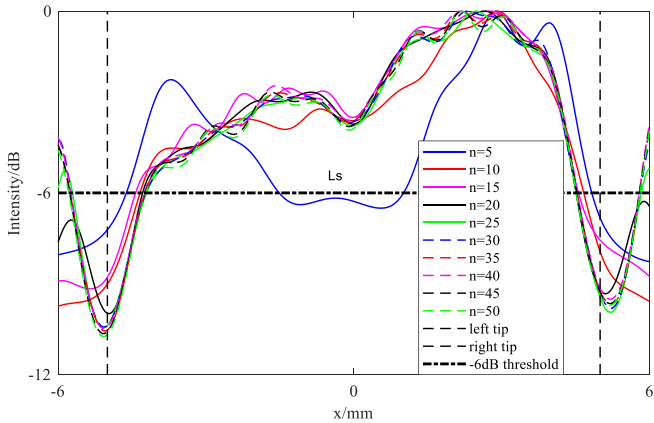


Fig. 9. Lateral cross sections through the peaks of PC-MUSIC images.

**Table 2**  
The assessed length for slot in steel sample.

n	Assessed length/mm	Error	Imaging time/s
5	/	/	12.4
10	9.038	0.962 (9.62%)	13.5
15	9.038	0.962 (9.62%)	14.1
20	8.837	1.163 (11.63%)	15.1
25	8.787	1.213 (12.13%)	15.6
30	8.787	1.213 (12.13%)	17.1
35	8.787	1.213 (12.13%)	17.6
40	8.837	1.163 (11.63%)	18.4
45	8.787	1.213 (12.13%)	19.4
50	8.787	1.213 (12.13%)	21.0

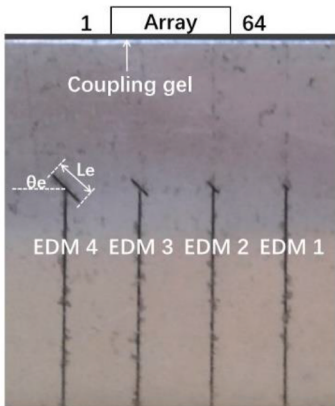


Fig. 10. Steel sample with EDM lines.

From Fig. 5(c) and (d), it is obvious that there are six peaks for both lateral curves, and they are marked as from 1 to 6. A parameter  $d$  has been defined and introduced to represent the distance between adjacent SDHs. For example,  $d_{12}$  represents the distance between the first and second SDHs.

The assessed distances between adjacent SDHs based on the TR-MUSIC and PC-MUSIC imaging results have been summarized in Table 1, and the error has also been calculated.

From Table 1, it can be concluded that the error for assessed distance obtained from TR-MUSIC and PC-MUSIC images is smaller than 8% in the analyzed case. And the overall performance of TR-MUSIC is better than that of PC-MUSIC when distinguishing the lateral adjacent point-like targets.

In addition, the effect of gird size on the imaging result is also considered. Here, the gird size is set to be 0.1 mm, 0.05 mm and 0.025

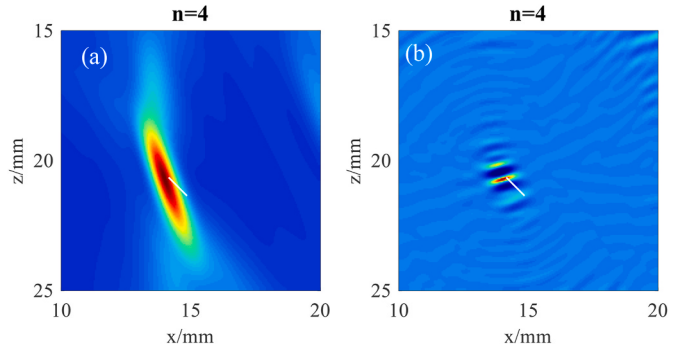


Fig. 11. (a) TR-MUSIC and (b) PC-MUSIC images for EDM1 (all images are displayed with -12dB dynamic range).

mm. Under different gird size, the lateral cross sections through the TR-MUSIC and PC-MUSIC images are shown in Fig. 6. And the corresponding imaging time is 3.52 s, 13.34 s and 55.82 s.

According to the result labelled 'TR-MUSIC' shown in Fig. 6, it can be observed that the lateral cross curves under different gird size coincide with each other, meaning that the TR-MUSIC is robust to the grid size. And based on the result labelled 'PC-MUSIC', it can be seen that when the gird size is set to be 0.025 mm, the corresponding curve has slightly difference with the other two curves, but the imaging time becomes much longer. So the gird size is not the main factor to effect location accuracy via comparing these curves. The grid size is set to be 0.05 mm in the imaging process.

Case two: Super resolution imaging for extended target.

Following the same process with case one, the ultrasonic array data are collected via FMC process and the scattered signals related with the slot are extracted in the signal preprocessing stage. The matrix  $K$  can be constructed via time-frequency transform of scattered signals. At each frequency component  $\omega$  over the frequency range from 1 MHz to 9 MHz, the SVD of  $K(\omega)$  is implemented, and the distribution of singular value amplitude (in dB) over the frequency range from 1 MHz to 9 MHz are shown in Fig. 7.

The distributed characteristic of singular values for slot is different with that for SDHs by comparing Figs. 4 and 7. There are no obvious singular values in the whole frequency bandwidth. It is hard to distinguish the signal subspace from the noise subspace directly. Therefore, various dimension of signal subspace  $n$  need to be considered in the imaging process to obtain the TR-MUSIC and PC-MUSIC images, and the size of grid is set to be 0.05 mm in the imaging area. Here,  $n = 5, 10, 15, 20, 25, 30, 35, 40, 45, 50$ , and only partial ultrasonic images are shown in Fig. 8. The rectangles in the ultrasonic images represent the position and actual size of slot.

Based on the TR-MUSIC images shown in Fig. 8(a), it can be observed that when  $n = 5$ , only some of the structural features of the slot can be extracted. In particular, the two peaks close to the slot tips. When  $n = 10, 15, 20, 30, 40$ , the area where the defect occurs can be determined, but it is much larger than the actual slot. Therefore, TR-MUSIC is not suited for characterization of extended target. Based on the PC-MUSIC images shown in Fig. 8(b), it is clear that PC-MUSIC images shows different characteristic with TR-MUSIC. When  $n = 5$ , only some of the structural features of the slot can be extracted. When  $n = 10, 15, 20, 30, 40$ , the whole slot can be detected, and its shape can also be distinguished. Therefore, PC-MUSIC images can be chosen to assess the length of slot. The lateral cross sections through the peaks of PC-MUSIC images are extracted and shown in Fig. 9.

The length of slot can be directly measured from its indication in an image, here, taking the 6 dB main lobe width as the assessed length  $L_s$ . Under different dimension of signal subspace, the assessed length can be obtained and summarized in Table 2. Note that the curve peaks for  $n = 5$  appear to not exactly correspond with the tips of slot, and the middle

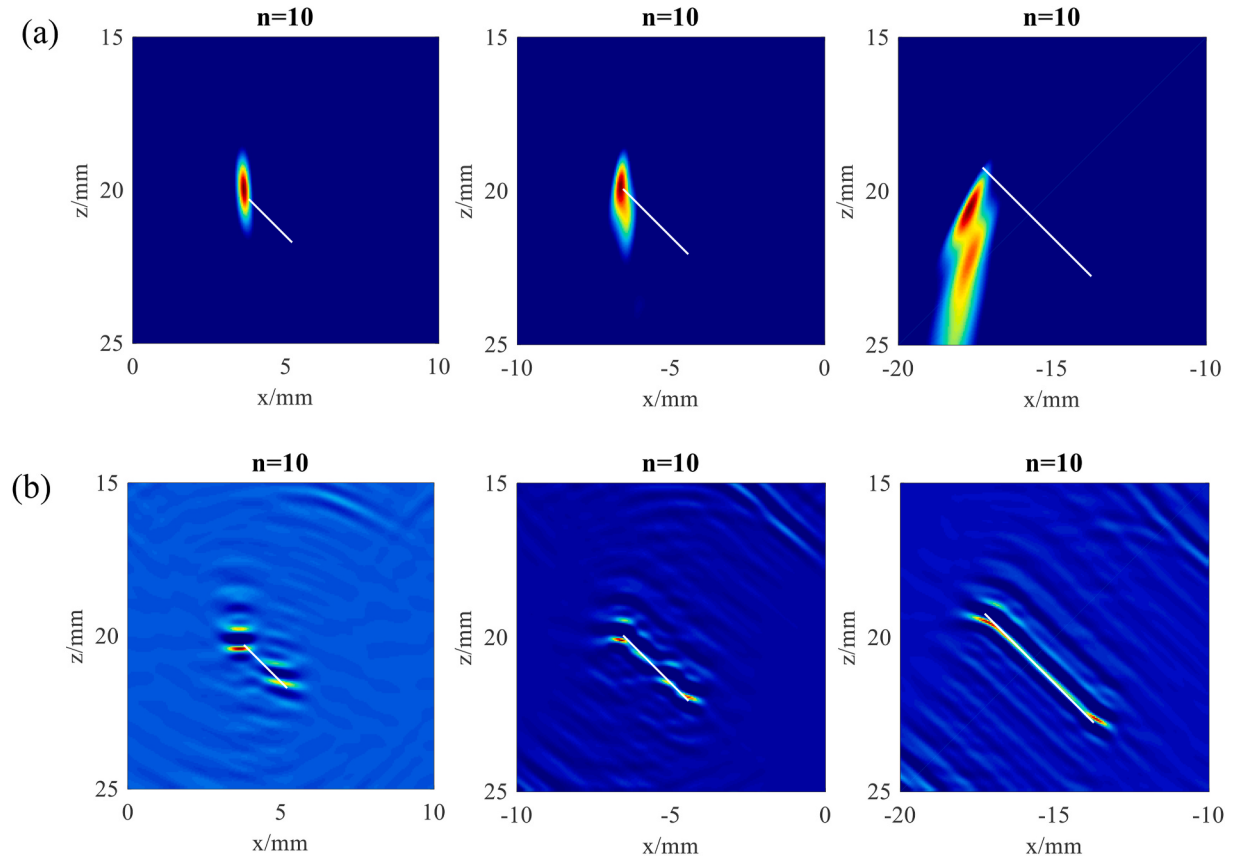


**Fig. 12.** (a)TR-MUSIC and (b) PC-MUSIC images for EDM2, EDM3 and EDM4 (all images are displayed with  $-12\text{dB}$  dynamic range).

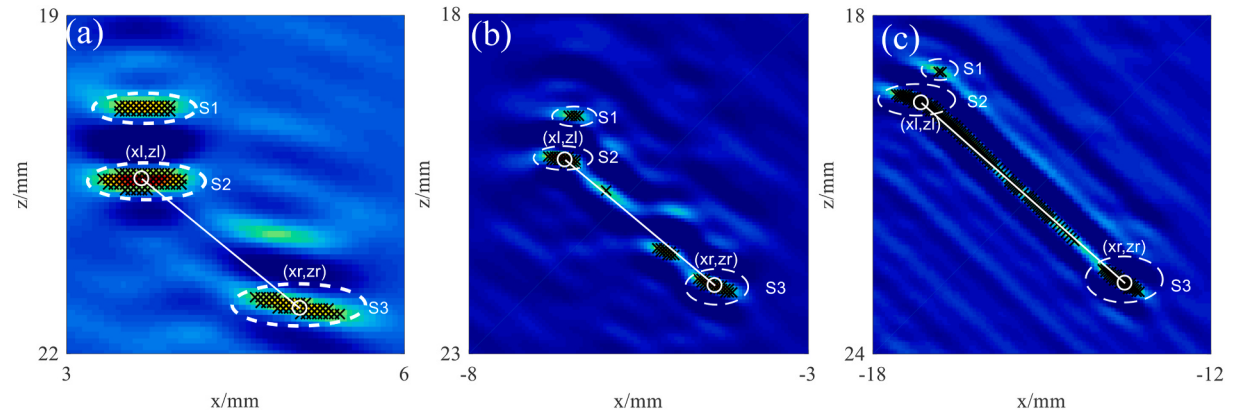


**Fig. 13.** Defect characterization based on PC-MUSIC images of (a) EDM2, (b) EDM3 and (c) EDM4 (all images are displayed with  $-12\text{dB}$  dynamic range).

part of the curve is below the  $-6\text{ dB}$  threshold, so the assessed length cannot be obtained for  $n = 5$  case. In addition, the imaging time is also provided.

From Table 2, it can be concluded that when  $n = 10$  and 15, the length of slot can be assessed with the error smaller than 9.62%. When  $n = 20, 25, 30, 35, 40, 45$  and 50, the error becomes larger, and the imaging time also becomes longer. The dimension of signal subspace can be set to be 10 and 15 to allow measurement of the length of the slot based on PC-MUSIC images, and the error is smaller. In addition, the larger the  $n$ , the longer the imaging time. Therefore, the dimension of signal subspace is set to be 10, and the error is 9.62% for the analyzed case. The future work will focus on the performance of PC-MUSIC for slots with different length and angle.

In summary, for lateral adjacent point-like targets (SDHs in the

experiment), both TR-MUSIC and PC-MUSIC can distinguish and locate the positon correctly, and the performance of TR-MUSIC is better than that of PC-MUSIC. For extended target (slot in the experiment), the division of signal and noise subspaces is different from that of point-like target, so various dimension of signal subspace is considered in the imaging process. TR-MUSIC can only determine the area where the defect occurs. PC-MUSIC can assess the length of defect under proper dimension of signal subspace, and the dimension of signal subspace is selected based on the error and imaging time for the given defect. Note that if  $n$  is too small, only the defect extremities can be located. If  $n$  is too large, the imaging time increased and there is little observable change in image characteristics compared to when  $n$  is medium. This will provide the preliminary suggestion for selection of  $n$ .

**Table 3**

The assessed length and angle for EDM lines.

	Assessed defect extremity/mm	Assessed length/mm	Error	Assessed angle/°	Error
EDM2	S2 (3.668, 20.45)	1.8172	0.1828 (9.14%)	39	6 (13.3%)
	S3 (5.075, 21.6)				
	S1 (3.668, 19.8)	2.2847	0.2847 (14.235%)	52	7 (15.6%)
	S3 (5.075, 21.6)				
EDM3	S2 (-6.583, 20.15)	2.8829	0.1171 (3.9%)	40	5 (11.1%)
	S3 (-4.372, 22)				
	S1 (-6.482, 19.5)	3.2714	0.2714 (9.04%)	50	5 (11.1%)
	S3 (-4.372, 22)				
EDM4	S2 (-17.14, 19.55)	4.8316	0.1684 (3.37%)	41.5	3.5 (7.78%)
	S3 (-13.52, 22.75)				
	S1 (-16.78, 19)	4.9689	0.0311 (0.62%)	49	4 (8.89%)
	S3 (-13.52, 22.75)				

### 3.2. Characterization of extended targets

A block of steel with four EDM lines is machined as shown in Fig. 10. The respective lengths are 1 mm for EDM1, 2 mm for EDM2, 3 mm for EDM3, 5 mm for EDM4. The central wavelength  $\lambda_c$  is 1.2 mm. Therefore, the EDM1 can be considered as the point-like target. The EDM2, EDM3 and EDM4 can be considered as the extended targets. In addition, all the EDM lines are oblique to the ultrasonic array, and the angle is 45°.

Following the same process as well as size of grid in the imaging area with section 3.1, the TR-MUSIC and PC-MUSIC images for EDM1 are obtained and shown in Fig. 11, and the lines in the ultrasonic images represent the position and actual size of the EDM1. Here, the dimension of signal subspace is set to be 4. In reality, the dimension of signal subspace is very important for correctly characterizing the extended target. However, there is no uniform rule to distinguish the signal subspace from the noise subspace so far.

It seems that both TR-MUSIC and PC-MUSIC can locate the position of left tip for EDM1. For PC-MUSIC, its imaging result for 1 mm EDM line is similar to that of 1 mm SDH. Therefore, PC-MUSIC have failed to distinguish the reflector, the length of which is smaller than the central ultrasonic wavelength, from a point-like target.

For EDM2, EDM3 and EDM4, the TR-MUSIC and PC-MUSIC are implemented to obtain the ultrasonic images shown in Fig. 12(a) and (b), and the line in each ultrasonic image represents the position and actual size of corresponding EDM line. Here, the dimension of signal subspace is set to be 10 and the grid size is set to be 0.05 mm in the imaging process. By comparing the TR-MUSIC and PC-MUSIC images, it can be concluded that TR-MUSIC only can detect the part of defects, specifically the left tip of EDM lines. PC-MUSIC can distinguish the shape of defects, and the imaging results can be utilized to assess the length and angle of these defects.

A sizing strategy has been introduced to achieve defect characterization as shown in Fig. 13. The detailed process has been followed, taking the EDM2 as an example.

Firstly, the position of image pixels (intensity  $\geq -6$  dB) have been searched based on the PC-MUSIC image, such as these pixels, the position of which labelled 'x', included in the area S1, S2 and S3.

Secondly, according to the characteristic of PC-MUSIC image, there are some false targets, which can be assessed and removed, such as these

pixels included in the area S1. Note that the false targets are identified via considering the characteristic of ultrasonic image as well as assessed errors for length and angle.

Thirdly, the area S2 and S3 correspond to the defect extremity. The position of peak for each area can be searched separately, and considered as the assessed defect extremity ( $xl, zl$ ) and ( $xr, zr$ ).

Lastly, according to the position of two assessed defect extremity, the assessed length  $L_e$  and angle  $\theta_e$  are calculated

$$L_e = \sqrt{|xl - xr|^2 + |zl - zr|^2}, \quad (6a)$$

$$\theta_e = \sin^{-1} \frac{|zl - zr|}{L_e} \quad (6b)$$

According to the sizing strategy, the assessed length and angle for EDM2, EDM3 and EDM4 are summarized in Table 3. Here, S1 and S2 are separately chosen to assess the defect extremity. By comparing the errors obtained from S1 and S2, it can be seen that the overall errors for length and angle when S2 is chosen are smaller than that when S1 is chosen, except for one case. Therefore, the pixels included in the area S1 can be considered as the false targets. When areas S2 and S3 are selected to assess the length and angle, it is clear that the error for length is smaller than 9.14% and the error for angle is smaller than 13.3% for the cases considered. The longer the length of defect, the smaller the error. Note that only the length and angle of regular EDM lines are chosen as the assessed parameters for defect characterization in this paper. More complex parameters are needed for the further practical applications.

### 4. Conclusion

This paper has described an investigation into the performance of time-reversal-based super resolution imaging technique for defect localization and characterization. Both TR-MUSIC and PC-MUSIC over a given frequency bandwidth are implemented to image the point-like and extended targets machined in metallic samples. Here, if the size of defect is smaller than the central ultrasonic wavelength, the defect can be regarded as point-like target. On the contrary, if the size of defect is larger than the central ultrasonic wavelength, it can be regarded as extended target. The principles for super resolution imaging and defect characterization based on ultrasonic super-resolved image have been introduced.

An experimental ultrasonic array system has been built to capture the real data from the test samples via FMC process. The first experiment was implemented on a block of steel with six 1 mm SDHs considered as the point-like targets, and one 10 mm slot considered as the extended target. For point-like targets, both TR-MUSIC and PC-MUSIC can distinguish and locate the positon correctly, and the performance of TR-MUSIC is better than that of PC-MUSIC for the case considered. For extended target, TR-MUSIC can only determine the area where the defect occurs. PC-MUSIC can assess the length of slot under proper dimension of signal subspace. The error as low as 9.62% can be achieved provided that optimum imaging parameters are applied, here, the dimension of signal subspace is set to be 10. And the error will become higher if non-optimum imaging parameters are applied. The second experiment was implemented on a block of steel with four EDM lines, one of which is considered as point-like target, and the other three are considered as extended targets. A defect sizing strategy based on the ultrasonic super-resolved image has also been utilized to obtain the length and angle of extended targets oblique to the array. The results show that PC-MUSIC can achieve defect characterization under proper dimension of signal subspace. The worst errors observed for length and angle were 9.14% and 13.3% respectively. And the errors were found to reduce with increasing defect length. Therefore, the PC-MUSIC can be further utilized to image more complex defect in the future.

## Author statement

Chengguang Fan has focused on the research on the ultrasonic time-reversal-based super resolution imaging. Sunquan Yu and Bin Gao have focused on the research on the defect characterization. Yong Zhao and Yei Yang have focused on the research on the experimental demonstration.

## Declaration of competing interest

The authors declare that they have no known competing financial interests or personal relationships that could have appeared to influence the work reported in this paper.

## Acknowledgment

This work was funded by the high-level innovative talent project of National University of Defense Technology.

## References

- [1] Drinkwater BW, Wilcox PD. Ultrasonic arrays for non-destructive evaluation: a review. *NDT&E Int* 2006;39:525–41.
- [2] Holmes C, Drinkwater BW, Wilcox PD. Post-processing of the full matrix of ultrasonic transmit-receive array data for non-destructive evaluation. *NDT&E Int* 2005;38:701–11.
- [3] Fink M. Acoustic imaging with time reversal methods: from medicine to NDT. *Rev Prog Quant Nondestr Eval* 2015;13:13–23.
- [4] Lev-Ari H, Devaney AJ. The time-reversal technique re-interpreted: subspace-based signal processing for multi static target location. *Proc IEEE Sensor Array and Multichannel Signal Processing Workshop* 2000:509–13.
- [5] Prada C, Thomas JL. Experimental subwavelength localization of scatterers by decomposition of the time reversal operator interpreted as a covariance matrix. *J Acoust Soc Am* 2003;114:235–43.
- [6] Simonetti F. Location of pointlike scatterers in solids with subwavelength resolution. *Appl Phys Lett* 2006;89:094105.
- [7] Marengo EA, Gruber FK, Simonetti F. Time-reversal MUSIC imaging of extended targets. *IEEE Trans Image Process* 2007;16:1967–84.
- [8] Labyed Y, Huang LJ. Ultrasound time-reversal MUSIC imaging of extended targets. *Ultrasound in Med. Ultrasound Med Biol* 2012;38:2018–30.
- [9] Asgedom E, Gelius LJ, Tygel M. Time-reversal multiple signal classification in case of noise: a phase-coherent approach. *J Acoust Soc Am* 2011;130:2024–34.
- [10] Labyed Y, Huang LJ. Super-resolution ultrasound imaging using a phase-coherent MUSIC method with compensation for the phase response of transducer elements. *IEEE Trans Ultrason Ferroelectrics Freq Control* 2013;60:1048–60.
- [11] He JZ, Yuan FG. Lamb wave-based subwavelength damage imaging using the DORT-MUSIC technique in metallic plates. *Struct Health Monit* 2016;15:65–80.
- [12] Yang XB, Wang K, Zhou PY, Xu L, Liu JL, Sun PP, Su ZQ. Ameliorated-multiple signal classification (Am-MUSIC) for damage imaging using a sparse sensor network. *Mech Syst Signal Process* 2022;163:108154.
- [13] Yang XB, Wang K, Zhou PY, Xu L, Su ZQ. Imaging damage in plate waveguides using frequency-domain multiple signal classification (F-MUSIC). *Ultrasonics* 2022;119:106607.
- [14] Xu CB, Wang JS, Yin SX, Deng MX. A focusing MUSIC algorithm for baseline-free Lamb wave damage localization. *Mech Syst Signal Process* 2022;164:108242.
- [15] Xu CB, Zuo H, Deng MX. Dispersive MUSIC algorithm for Lamb wave phased array. *Smart Mater Struct* 2022;31:025033.
- [16] Achenbach JD. Quantitative nondestructive evaluation. *Int J Solid Struct* 2000;37:13–27.
- [17] Felice MV, Fan Z. Sizing of flaws using ultrasonic bulk wave testing: a review. *Ultrasonics* 2018;88:26–42.
- [18] Elliott JB, Lowe MJS, Huthwaite P, Phillips R, Duxbury DJ. Sizing subwavelength defects with ultrasonic imagery: an assessment of super-resolution imaging on simulated rough defects. *IEEE Trans Ultrason Ferroelectrics Freq Control* 2019;66:1634–48.
- [19] Fan CG, Yang L, Zhao Y. Ultrasonic multi-frequency time-reversal-based imaging of extended targets. *NDT&E Int* 2020;113:102267.
- [20] Fan CG, Yang L, Zhao Y. Preprocessing of the full matrix capture data for time-reversal-based super-resolution imaging. *Insight* 2017;59:586–90.
- [21] Fan CG, Pan MC, Luo FL. Ultrasonic broadband time-reversal with multiple signal classification imaging using full matrix capture. *Insight* 2014;56:487–91.
- [22] Kerbrat E, Prada D, Cassereau D, Fink M. Imaging in the presence of grain noise using the decomposition of the time reversal operator. *J Acoust Soc Am* 2003;113:1230–40.
- [23] Fleming M, Lowe MJS, Simonetti F, Cawley P. Super resolution imaging: performance studies. *Rev Prog Quant Nondestr Eval* 2006;820:736–43.
- [24] Simonetti F. Multiple scattering: the key to unravel the subwavelength world from the far-field pattern of a scattered wave. *Phys Rev E* 2006;73:036619.
- [25] Velichko A, Wilcox PD. An analytical comparison of ultrasonic array imaging algorithms. *J Acoust Soc Am* 2010;127:2377–84.
- [26] Chiao RY, Thomas LJ. Analytic evaluation of sampled aperture ultrasonic imaging techniques for NDE. *IEEE Trans Ultrason Ferroelectrics Freq Control* 1994;41:484–93.
- [27] Sakhai M, Mahloojifar A, Malek A. Optimization of point spread function in ultrasound arrays. *Ultrasonics* 2006;44:159–65.
- [28] Zhang J, Drinkwater BW, Wilcox PD. The use of ultrasonic arrays to characterize crack-like defects. *J Nondestr Eval* 2010;29:222–32.
- [29] Peng CY, Bai L, Zhang J, Drinkwater BW. The sizing of small surface-breaking fatigue cracks using ultrasonic arrays. *NDT&E Int* 2018;99:64–71.